NeuroImage: Clinical 23 (2019) 101894

Contents lists available at ScienceDirect

NeuroImage: Clinical

journal homepage: www.elsevier.com/locate/ynicl

Neuroimaging of the component white matter connections and structures within the cerebellar-frontal pathway in posterior fossa tumor survivors

Alyssa S. Ailion[a], Simone Renée Roberts[a,c,d], Bruce Crosson[a,b,c,d], Tricia Z. King[a,*]

[a] Department of Psychology, the Neuroscience Institute, Georgia State University, United States of America
[b] Department of Radiology and Imaging Sciences, Emory University School of Medicine, United States of America
[c] Department of Neurology, Emory University School of Medicine, United States of America
[d] Atlanta VA Center of Excellence for Visual and Neurocognitive Rehabilitation, United States of America

ARTICLE INFO

Keywords:
Brain tumor
Structural MRI
Diffusion tractography
Cerebellum
White matter pathway
Brain volume
White matter
Voxel-based morphometry
Cerebellar atrophy

ABSTRACT

Introduction: In posterior fossa tumor survivors, lower white matter integrity (WMI) in the right cerebellar-left frontal pathway has been well documented and appears to be related to proximity to the cerebellum, radiation treatment, as well as time since treatment in both cranial radiation and surgery-only treatment groups. The current study investigated theories of transneural degeneration following cerebellar tumor resection that may underlie or relate to reductions in WMI and regional brain volumes using correlations. We hypothesized a positive relationship between the volume of the right cerebellum and known white matter output pathways, as well as with the volume of structures that receive cerebellar projections along the pathway.

Methods: Adult survivors of childhood brain tumors were recruited (n = 29; age, M = 22 years, SD = 5; 45% female). Age- and gender-matched controls were also included (n = 29). Participants completed 3 T diffusion-weighted and T1 MPRAGE MRI scans. Brain structure volume relative to intracranial vault served as regional volumetric measures. Fractional anisotropy (FA) and radial diffusivity (RD) served as WMI measures. In the survivor group, partial correlations between WMI and regional volume included controlling for disease severity.

Results: In posterior fossa tumor survivors, the volumes of the cerebellum, thalamus, and frontal lobe were correlated with WMI of the thalamic-frontal segment of the cerebellar-frontal pathway (r = 0.41–0.49, $p < .05$). Cerebellar atrophy was correlated with reduced WMI in the cerebellar-rubral segment (FA, $r = -0.32$ $p > .05$; RD, $r = 0.53$, $p < .01$). In the no-radiation survivor group, the regional volume of each structure along the pathway was associated with WMI in the cerebellar-rubral segment. In the radiation survivor group, significant correlations were found between the regional brain volume of each structure and the thalamic-frontal segment of the pathway.

Discussion: The results of this multimodal neuroimaging study provide correlational evidence that the mechanism of injury subsequent to brain tumor treatment may be different depending on type of treatment(s). Without radiation, the primary mechanism of injury is cerebellar tumor growth, resection, and hydrocephalus. Therefore, the most proximal connection to that injury (cerebellar-rubral pathway) was correlated with reductions in volume along the pathway. In contrast, the survivor group treated with radiation may have had possible radiation-induced demyelination of the thalamic-frontal portion of the pathway, based on a strong correlation with volume loss in the cerebellum, red nucleus, thalamus, and frontal lobe.

1. Introduction

Cerebellar brain tumors account for about 20% of all childhood tumors, and the majority of children survive (Gurney et al., 1999; Ostrom et al., 2015). However, poor neurocognitive and neuroanatomical outcomes often are associated with survivorship (Ailion et al., 2017; Duffner, 2004). Most cerebellar tumors occur in early childhood during important periods of brain maturation (Mueller and Chang, 2009; Nejat et al., 2008; Ostrom et al., 2015). During this sensitive period for brain development, young children are treated with resection, radiation, chemotherapy, and shunts, all of which are based on age at presentation, location, malignancy, and intracranial pressure. However, many benign tumors require gross total resection followed by no adjuvant treatment at all (Mueller and Chang, 2009).

* Corresponding author at: Department of Psychology, Georgia State University, P.O. Box 5010, Atlanta, GA 30302-5010, United States of America.
E-mail address: tzking@gsu.edu (T.Z. King).

https://doi.org/10.1016/j.nicl.2019.101894
Received 1 February 2019; Received in revised form 7 May 2019; Accepted 8 June 2019
Available online 10 June 2019

The cerebellum is of particular interest because estimates suggest that 82–84% of all neurons reside in the cerebellum, despite the cerebellum being only about 11% of the total brain volume (Andersen et al., 1992; Lange, 1975). Furthermore, the cerebellar hemispheres are structurally connected and functionally related to the coordination between the cerebellum and the cortex via reciprocal pathways that project through the red nucleus and thalamus to the cortex (Alexander et al., 1986; Blumenfeld, 2010; Kelly and Strick, 2003; Parent, 1996). Thus, researchers have called for a more integrated view of the brain that accounts for the structural and functional role of the cerebellum in coordination with the cortex (Herculano-Houzel, 2009; Whiting and Barton, 2003).

Prior studies on brain tumor survivors have documented damage to the brain structures involved the cerebellar-frontal pathways, including reduced volume in the hemispheres, vermis, and dentate of the cerebellum (Puget et al., 2009; Kirschen et al., 2008; Konczak et al., 2005; Küper et al., 2013), lower white matter integrity (WMI) in the pons (Khong et al., 2003; Morris et al., 2009), and lower volume in the thalamus bilaterally (Zhang et al., 2008). Cerebellar atrophy also has been found in cerebellar tumor survivors (Ailion et al., 2016; Dietrich et al., 2001; Szathmari et al., 2010). Furthermore, a number of researchers have reported lower WMI in the frontal lobe (King et al., 2015; Qiu et al., 2007; Soelva et al., 2013). Lower WMI in the frontal lobe has been found in survivors regardless of radiation treatment (Rueckriegel et al., 2015), but for survivors treated with radiation, frontal lobe WMI has appeared to be uniquely vulnerable when compared to parietal lobe WMI (Qiu et al., 2007).

One study of cerebellar atrophy following traumatic brain injury (TBI) highlights the relationships among the volumes of the cerebellum, pons, thalamus, and dorsolateral prefrontal cortex. Spanos et al. (2007) inferred based on their volumetric results from morphometry that the cerebellum and corresponding regions included in cerebellar-cortical pathways, particularly the pons and the dorsolateral prefrontal cortex, may be vulnerable to a cascading impact of cerebellar atrophy following a moderate to severe TBI. The authors proposed that cerebellar atrophy may be related to lower regional volume in the other brain regions in the cerebellar-frontal pathways per structural dissociation due to myelin or axonal degeneration, however this theory was never tested (Spanos et al., 2007). As the authors mention in their conclusion, diffusion tractography could be used to construct the cerebellar-frontal pathway to test whether measures of myelin or axon degeneration are correlated with lower regional volume within these brain structures.

The cerebellar-frontal pathway has been of particular interest in the childhood cerebellar tumor population because this population has lower WMI in the frontal-cerebellar pathways bilaterally when compared to controls (Law et al., 2011; Law et al., 2015a; Soelva et al., 2013). Correspondingly, lower WMI in the right cerebellar-left frontal pathway has been correlated with cerebellar resection and radiation treatment (Law et al., 2011; Law et al., 2015a; Law et al., 2015b); this finding applies to survivors treated with cranial radiation and those treated with only surgical resection (Law et al., 2011). Furthermore, longer time since treatment correlated with lower WMI in the right cerebellar-left frontal pathway regardless of treatment (e.g., surgery alone vs. radiation; Law et al., 2011; Law et al., 2015a). Within the right cerebellar-left frontal pathway, posterior segments (e.g., cerebellar-rubral) had lower WMI when compared to other segments (e.g., rubral-thalamic and thalamic-cortical), which was attributed to both surgery and radiation (Law et al., 2015a). Taken together, lower WMI in the right cerebellar-left frontal pathway has been well documented and appears to be related to the segment of the pathway and radiation treatment, as well as time since treatment, in both cranial radiation and surgery-only treatment groups.

One explanation for lower regional volume and WMI within the brain regions of the cerebellar-frontal pathways originates in the functional neuroimaging literature. Theories of brain function suggest that a lesion can disrupt neural activity, which in turn disrupts functional connections between the lesioned region and its distant functional connections, a concept known as diaschisis (von Monakow, 1914). One functional imaging study reported that diaschisis occurs in the forebrain after stroke in the cerebellum (Rehme and Grefkes, 2013). In terms of brain structure, transneural degeneration refers to the structural death at the cellular level following brain injury due to structural disconnection among the pre- and post- synaptic neurons, which subsequently underlies functional diaschisis (Deleglise et al., 2018; Eisen and Weber, 2001; Koliatsos et al., 2004; Pinching and Powell, 1971). Therefore, possible transneural degeneration following cerebellar tumor resection and subsequent cancer treatment may underlie or relate to reductions in WMI and volume in the brain structures involved in the cerebellar-frontal pathway.

To review, prior literature provides evidence for 1) reduced volume in the brain structures involved in the cerebellar-frontal pathway following cerebellar tumor treatment, 2) reduced volume in the brain structures involved in the cerebellar-frontal pathway following cerebellar atrophy, 3) reduced WMI within the cerebellar-frontal pathway following cerebellar tumor treatment, and 4) theories which support possible transneural degeneration within the cerebellar-frontal pathway. While prior research has investigated the WMI of the cerebellar-frontal pathway (e.g., Law et al., 2015a) and volumetric measures of brain structures along this pathway (e.g., Kirschen et al., 2008), no study has combined diffusion-based metrics and volumetric measures to determine the relationships between regional brain volumes and the individual pathways that connect the regions in brain tumor survivors. In addition to substantial empirical evidence, theories suggesting vulnerability to structural and functional connections within the cerebellar-frontal network support the rationale for testing these relationships.

The goal of the current study was to test the neuroanatomical relationships among brain regions and the individual pathways that connect them. We hypothesized a positive relationship between the volume of the right cerebellum and known white matter output pathways (i.e., cerebellar-rubral, cerebellar-thalamic, rubral-thalamic, and thalamic-frontal), as well as the volume of structures that receive cerebellar projections along the pathway (right dentate, left red nucleus, left thalamus, and left frontal lobe). Furthermore, the regional volume of brain structures that receive cerebellar output should have positive relationships with the WMI of connected pathways (e.g., left red nucleus volume would be related to rubral-thalamic WMI; See Fig. 1). Similarly to the first hypothesis, cerebellar atrophy should be negatively correlated with WMI in each segment (cerebellar-rubral, cerebellar-thalamic, rubral-thalamic, and thalamic-frontal).

2. Methods

Data for the current study was obtained from a larger study on the long-term neuropsychological outcomes following pediatric brain tumor diagnosis and treatment (PI: T.Z. King #RSGPB-CPPB-114044). The current paper focuses on exclusively on treatment-related factors and their impact on structural neuroanatomical connectivity within the individual white matter segments and brain structures within the cerebellar-frontal pathway. We conducted a concurrent study which investigates the relationship between neuropsychological constructs and their distinct neuroanatomical basis using neuroimaging metrics. The same sample (29 adult survivors of cerebellar tumor and 29 neurotypical matched controls) and neuroimaging methods were employed in both studies. This manuscript is distinct because it takes a statistical approach to answer questions about how treatment relates to structural connectivity, whereas our other study explored the relations of specificity between brain structure and neuropsychological function in the same cohort.

Detailed methods and study procedures are described by King et al. (2015b) and Ailion et al. (2016). In brief, survivors either were part of a long-term follow-up of a prior longitudinal study of childhood brain

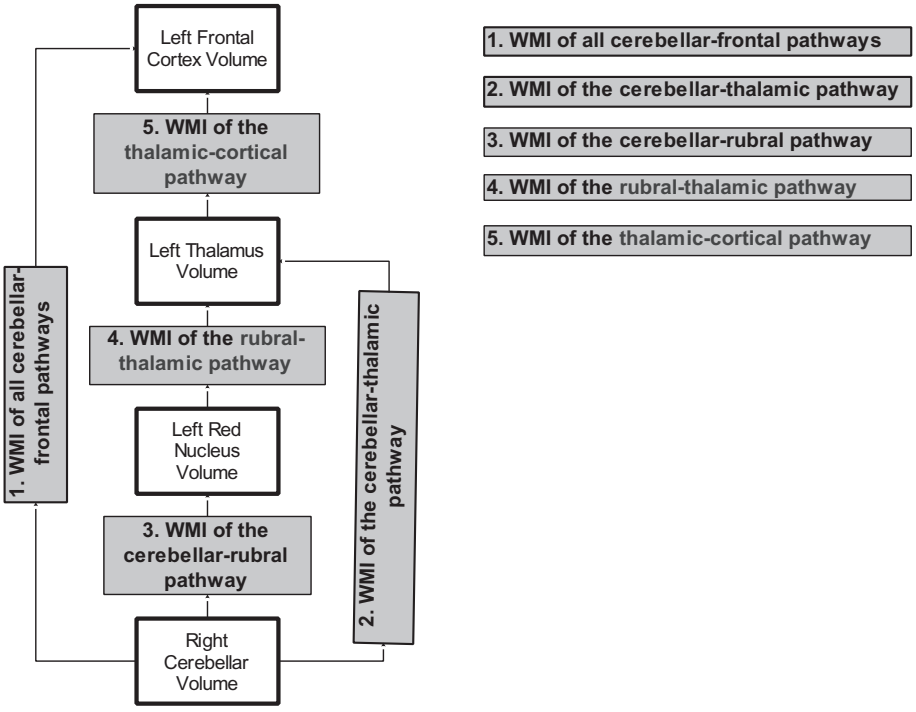

Fig. 1. Hypothesized relationships between brain structure volumes and white matter pathways in the cerebellar-frontal network.
Note. WMI = White matter integrity; White boxes represent the volume of structures in the brain, and grey boxes represent the white matter pathways that connect the structures in the brain.

tumors, or recruited from a database of brain tumor survivors obtained from Children's Healthcare of Atlanta (CHOA). Control participants were recruited from the Georgia State University community through the psychology participant pool, fliers posted around the community, and the Georgia State University/Georgia Institute of Technology Joint Center for Advanced Brain Imaging (CABI). The Georgia State University (IRB# H03177) and Georgia Institute of Technology (IRB# H14088) Institutional Review Boards reviewed and approved all studies.

A total of 44 participants with tumors in the cerebellum, brain stem, or posterior fossa completed the study. Participants were excluded based on the following criteria: global functional impairment (n = 2), pervasive developmental disorder (n = 1), English as a second language (n = 1), < 5 years from diagnosis (n = 1), or younger than 16 years old at exam (n = 6). Survivors were matched with controls on demographic factors that included age, sex, level of education, and handedness. The total sample included 29 survivors and 29 controls with neuroimaging data for processing (Tables 1 and 2).

The 29 survivor participants were on average 8.55 years old (SD = 4.88; range 0–18) at diagnosis, and their average age at exam was 21.34 years (SD = 5.35; range 16–35). The average Full-Scale IQ (Wechsler Abbreviated Scale of Intelligence-2; WASI; Wechsler, 1999) was 99.07 (SD = 13.32). Thirteen individuals were diagnosed with astrocytoma tumors, 12 with medulloblastoma, and the remaining 4 individuals were diagnosed with an ependymoma, a glioma, a primitive neuroectodermal tumor (PNET) - not otherwise specified, and a choroid plexus tumor. Reported ethnicity in the sample was 72% Caucasian, 14% African-American, 7% Hispanic, and 7% Asian. With regard to treatment history, 83% of the sample had hydrocephalus, 52% had radiation treatment (RT), 48% had chemotherapy (only 1 participant had chemotherapy without RT), 55% had a hormone deficiency, and 3% had a seizure disorder. None of the survivors had posterior fossa syndrome listed in their medical chart, however 4 survivors (14%) were noted to have a “speech disorder.” Of those who had RT (n = 15), 80% had whole brain RT and an additional focal boost to the posterior fossa, the remaining 20% of participants (n = 3) received only focal RT. RT dosage ranged from 5040 to 6300. Treatment protocol numbers included: 9961 Arm A (n = 2), CCG 9961 Arm A (n = 3), CCG 9961 Reg B (n = 1), CCG 9892 (n = 1), CCG 88703-NOS (n = 1), POG 8633 (n = 1), POG 8695 (n = 1), POG 8930 (n = 1), ACNS 0331 (n = 1), and three participants did not have protocol numbers listed in their medical charts.

Participants completed an MRI scan using a 3-Tesla Siemens Trio system and a standard 12 channel head coil, which included a sagittally acquired, T1-weighted MPRAGE image (FOV = 256 mm, voxel size = 1x1x1mm, TR/TE = 2250 ms/3.98 ms, flip angle = 9°), a diffusion-weighted, spin-echo echo planar imaging (EPI) sequence with 30 gradient directions acquired along the anterior-to-posterior phase encoding direction (FOV = 204 mm, voxel size = 2x2x2mm, TR/TE = 7700 ms/90 ms, flip angle = 90°, b = 1000s/mm^2, GRAPPA parallel imaging acceleration factor = 2, number of slices = 60), and one un-weighted diffusion volume (b = 0 s/mm^2). The DWI sequence lasted 8 min and 22 s. The same method described for a prior DWI study with this sample (Smith et al., 2016) was used to co-register the diffusion image and the T1 image using the fMRI data and field map. The co-registration method used the fMRI sequence aquired in the same session as the T1 and DWI sequence (FOV = 204 mm, voxel size = 3x3x3mm, TR/TE = 2130 ms/30 ms, flip angle = 90°, number of slices = 40, slice gap = 0, EPI = 180 volumes), and corresponding fMRI field map (FOV = 204 mm, voxel size = 3x3x3mm, TR/TE1/TE2 = 488 ms/4.92 ms/ 7.38 ms, flip angle = 60°) to apply the estimated phase shift to the diffusion scan. Three survivors and two controls with 1–10 DWI volumes containing artifact were corrected by removing those volumes from the dataset. The preprocessing pipeline included linear eddy current and motion correction (FDT FMRIB's Diffusion Toolbox FSL 5.0), skull stripping, tensor model fitting using FDT's DTIFIT, and co-alignment of DWI and T1 images using the fMRI field map.

The cerebellar-frontal pathway was constructed based on 5 regions of interest (ROIs): right cerebellar hemisphere, right dentate, left red nucleus (RN), left thalamus, and left middle frontal gyrus (MFG). While

Table 1
Survivor and control demographic and descriptive comparisons.

	Survivors $n = 29$	Controls $n = 29$	Group differences	Cohen's D
Gender	45% Female	48% Female		
Age at exam (years)	$M = 21.34$ $SD = 5.35$	$M = 22.43$ $SD = 5.20$	$t = 0.79$, $p = .56$	−0.02
Years of education	$M = 13.28$ $SD = 2.79$	$M = 14.34$ $SD = 2.79$	$t = -1.77$, $p = .08$	−0.38
Age at diagnosis (years)	$M = 8.55$ $SD = 4.88$ Range 1–18			
Radiation	$n = 15$ 52%			
Chemotherapy	$n = 14$ 48%			
High grade tumor	$n = 14$ 48%			
Hydrocephalus	$n = 24$ 83%			
Seizure medication	$n = 1$ 3%			
Hormone deficiency	$n = 16$ 55%			
Whole brain grey matter volume**	$M = 0.77$ $SD = 0.05$	$M = 0.81$ $SD = 0.02$	$t = 4.04$, $p < .01$	−1.05
Whole brain white matter volume*	$M = 0.31$ $SD = 0.02$	$M = 0.32$ $SD = 0.02$	$t = 2.46$, $p = .02$	−0.50
Right cerebellar volume	$M = 0.10$ $SD = 0.03$	$M = 0.10$ $SD = 0.05$	$t = 0.54$, $p = .59$	0.00
Right dentate volume	$M = 0.04$ $SD = 0.02$	$M = 0.04$ $SD = 0.03$	$t = 0.60$, $p = .55$	0.00
Left red nucleus volume	$M = 0.03$ $SD = 0.02$	$M = 0.04$ $SD = 0.03$	$t = 0.45$, $p = .65$	−0.39
Left thalamus volume	$M = 0.04$ $SD = 0.02$	$M = 0.04$ $SD = 0.03$	$t = -0.05$, $p = .96$	0.00
Left frontal volume	$M = 0.07$ $SD = 0.02$	$M = 0.06$ $SD = 0.03$	$t = -0.67$, $p = .51$	0.39
Cerebellar-frontal FA	$M = 0.32$ $SD = 0.06$	$M = 0.32$ $SD = 0.05$	$t = -0.04$, $p = .97$	0.00
Cerebellar-frontal RD**	$M = 0.0013$ $SD = 0.0003$	$M = 0.0011$ $SD = 0.0001$	$t = -2.64$, $p < .01$	0.89

Note. ** indicates $p < .01$ and * indicates $p < .05$; All volume measures are regional grey matter plus white matter divided by intracranial vault.

prior tractography studies defined the frontal ROI as the entire frontal lobe, the current study refined this region by including more specific anatomical boundaries within the frontal lobe (BA 46; Brodmann, 1909; Catani et al., 2012; Desikan et al., 2006; Turken and Dronkers, 2011). The dorsolateral prefrontal cortex (BA 46) was selected as the region within the frontal lobe because BA 46 received input from the cerebellum based on an animal virus tracing study (Kelly and Strick, 2003), and was associated with working memory performance in human fMRI studies (Marvel and Desmond, 2010; Zhang, Leung, and Johnson, 2003). The gyral region best corresponding to BA 46 was estimated using sulci boundaries of the rostral division of the MFG (Catani et al., 2012; Desikan et al., 2006). The boundaries included the anterior portion of the superior frontal sulcus, caudal portion of the MFG, dorsal boundary as the superior frontal sulcus, and ventral boundary as the inferior frontal sulcus (Catani et al., 2012; Desikan et al., 2006). For additional information on how regions of interest were defined, please see the Appendix A.

The tractography fiber reconstruction methods described below are based on the deterministic tractography pipeline developed by Roberts (2017), which was modeled after the methods of Ford et al. (2013) and Bohsali et al. (2015). TrackTools, a software suite developed in Dr. Thomas Mareci's research lab at the University of Florida, was used to globally reconstruct white matter pathways by characterizing MR signal attenuation according to a Mixture of Wisharts (MOW) probability distribution and applying a spherical deconvolution algorithm (MRI Analysis Software (MAS) http://marecilab.mbi.ufl.edu; Jian & Vemuri, 2007a, 2007b; Jian et al., 2007), prior to filtering estimated pathways to exclude streamlines that do not directly connect ROIs in a structural network (Colon-Perez et al., 2015). Network tractography was completed using PanTrack (a software suite developed by co-author SR; http://www.pantrack.org), which generates comprehensive structural networks with streamlines both between and within ROIs (see Appendix B of Roberts, 2017).

Global tractography files were generated using TrackTools. Fiber estimations were launched bi-directionally at a step interval of 0.25 mm. Tracking ceased when the angular deviation exceeded 65°. The optimal parameters for the angular deviation and step length were

Table 2
Subgroup descriptive statistics and effect sizes.

	Subgroup descriptive statistics			Subgroup differences Cohen's D		
	No Radiation $n = 14$ M (SD)	Radiation $n = 15$ M (SD)	Controls $n = 29$ M (SD)	No Radiation vs. Radiation	No Radiation vs. Controls	Radiation vs. Controls
Gender	43% Female	47% Female	48% Female			
Age at exam (years)	20.86 (4.96)	21.43 (5.72)	22.43 (5.20)			
Years of education	13.43 (2.68)	13.00 (2.94)	14.34 (2.79)			
Age at diagnosis (years)	9.64 (5.29) Range 1–18	7.00 (4.82) Range 1–17				
Radiation	$n = 0$ 0%	$n = 15$,100%				
Chemotherapy	$n = 1$ 7%	$n = 13$ 87%				
Hydrocephalus	$n = 11$ 79%	$n = 13$ 87%				
Shunt	$n = 3$ 21%	$n = 5$ 33%				
Seizure medication	$n = 1$ 7%	$n = 0$ 0%				
Hormone deficiency	$n = 1$ 7%	$n = 15$,100%				
Global grey matter volume	0.78 (0.04)	0.77 (0.06)	0.81 (0.02)	0.19	−1.07	−1.04
Global white matter volume	0.31 (0.02)	0.31 (0.03)	0.32 (0.02)	0.00	−0.50	−0.42
Right cerebellar volume	0.11 (0.02)	0.09 (0.02)	0.10 (0.05)	0.78	0.50	−0.42
Right dentate volume	0.04 (0.02)	0.04 (0.02)	0.04 (0.03)	0.00	0.00	0.00
Left red nucleus volume	0.03 (0.02)	0.03 (0.02)	0.04 (0.03)	0.00	−0.37	−0.37
Left thalamus volume	0.05 (0.02)	0.04 (0.01)	0.05 (0.03)	0.64	0.00	−0.40
Left frontal volume	0.07 (0.02)	0.07 (0.02)	0.06 (0.03)	−0.40	0.00	0.37
Cerebellar atrophy	9.57 (14.83)	12.47 (13.70)	–	−0.20	–	–
Cerebellar-frontal FA	0.32 (0.05)	0.32 (0.07)	0.32 (0.05)	0.00	0.00	0.00
Cerebellar-frontal RD	0.0012 (0.0002)	0.0013 (0.0003)	0.0011 (0.0001)	−0.39	0.72	1.04

Note. All volume measures are grey matter plus white matter divided by intracranial vault; Cohen's D: Small = 0.2–0.3, Medium = 0.5*, Large ≥0.8**; FA = fractional anisotropy; RD = radial diffusivity.

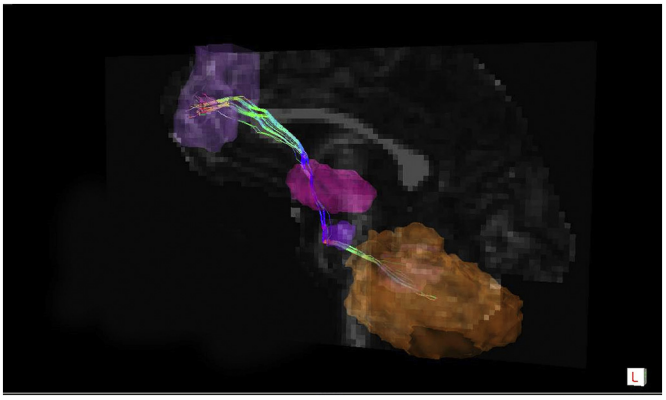

Fig. 2. Right Cerebellar– Left Frontal Pathway.
Note: Fibers displayed are filtered through the right cerebellum (orange), right dentate (pink outline within orange ROI), left red nucleus (light purple), left thalamus (pink), and left middle frontal gyrus (light purple).

informed by previous research (Bohsali et al., 2015) but determined ad hoc. PanTrack was used for network tractography to generate all of the direct connections between the right cerebellum and the left MFG. PanTrack output was then viewed in TrackVis. Each pathway was qualitatively confirmed for every participant, prior to manual filtering and applying streamline exclusions. The cerebellar-frontal pathway was defined as streamlines that began in the right cerebellum and continued to the left RN, left thalamus, and terminated in the left MFG (see Fig. 2). Streamlines that crossed through the corpus callosum were excluded. TrackTools was used to create a voxel-based mask (1x1x1mm^3) of the cerebellar-frontal tract. Lastly, FA and RD values were extracted for each pathway mask using FSLmeants. Deterministic tractography was used to compute fractional anisotropy (FA) and radial diffusivity (RD) for each component segment of the cerebellar-frontal pathway (i.e., cerebellar-rubral, rubral-thalamic, and thalamic-frontal).

Methods described in Ailion et al. (2016) were used to compute whole brain volume using Voxel-Based Morphometry. In brief, voxel-based morphometry (VBM) was used to compute the volume of each structure (right cerebellar hemisphere, right dentate, left red nucleus, left thalamus, and left middle frontal gyrus (MFG)) relative to the intracranial vault. Atrophy was calculated as described by Ailion et al. (2016).

The Neurological Predictor Scale (NPS; King and Na, 2016; Micklewright et al., 2008; Taiwo, Na, and King, 2017) was used as a cumulative measure of treatment complications such as hydrocephalus, hormone deficiency, seizures, and treatment (i.e., surgery, RT). Treatment severity was computed based on the Neurological Predictor Scale (NPS; Micklewright et al., 2008). The average NPS score for the sample was 6 (SD = 2.54; Range 2–9).

Pearson correlations were used to test relationships between the volume of the right cerebellum and the known white matter output pathways (i.e., cerebellar-rubral, rubral-thalamic, and thalamic-frontal), as well as the volume of structures that receive cerebellar output along the pathway (i.e., left red nucleus, left thalamus, and left frontal lobe). Correlations were computed to test for possible cascading damage, such that each of the following metrics would be positively correlated with one another: cerebellar-rubral WMI ➔ left red nucleus volume ➔ rubral-thalamic WMI, rubral-thalamic WMI ➔ left thalamus volume, and thalamic-frontal WMI ➔ left frontal volume. In contrast, non-cascading damage would be statistically represented by focal relationships among specific regions (i.e., left red nucleus, cerebellum, and thalamus all related only to thalamic-frontal WMI).

The theoretically driven hypotheses yielded 50 analyses for each scalar metric of WMI (i.e., FA and RD). An additional 32 analyses of FA and RD were run post hoc to explore the relationship between radiation treatment, volumetric measures, and scalar metrics of WMI. The Benjamini-Hochberg statistical correction for family-wise error was used with the recommended 5% false positive rate to correct for multiple comparisons, and all reported analyses survived statistical correction (Benjamini and Hochberg, 1995; Bennett et al., 2009). All of the values ranged from 0.00–0.05; all significant p values achieved a Benjamini-Hochberg critical value of < 0.01. The statistical correction was determined by rank ordering the p-values for all analyses and computing the Benjamini-Hochberg critical value using the following formula:

$$\text{Benjamini} - \text{Hochberg critical value} = (i/m) * Q$$

$$i = \text{the individual p} - \text{value rank } (1 - 100)$$

$$m = \text{total number of tests } (100)$$

Q = the false discovery rate (5%)

Assumptions for analyses were tested for each dependent variable (e.g., normality, homogeneity of variance), and no variables violated the assumptions of parametric tests.

3. Results

Cerebellar volume was only significantly correlated with the WMI of the most distal portion of the cerebellar-frontal pathway, the thalamic-frontal segment, in the survivor group (see Table 3). These correlations continued to be significant after correcting for treatment factors. For the control group, none of the hypothesized relationships reached statistical significance. However, small to medium Pearson correlation coefficients (r = −0.18–0.35) were observed for the cerebellar-rubral and rubral-thalamic segments in the control group.

For the survivor group, the FA and RD of the thalamic-frontal segment were associated with both thalamic volume and frontal lobe volume. These results are consistent with the study conducted by Law et al. (2015a) that found lower WMI in the cerebellar-rubral and thalamic-frontal segment of the cerebellar-frontal pathway. These relationships remained significant after controlling for treatment factors. In the control group, only the RD of the rubral-thalamic segment of the cerebellar-frontal pathway was associated with the volume the red nucleus and the thalamus. These results were inconsistent with the

Table 3
Correlations between cerebellar volume and the diffusion-based scalar metrics of the segments of the cerebellar-frontal white matter pathway.

	Cerebellar-rubral		Rubral-thalamic		Thalamic-frontal	
	FA	RD	FA	RD	FA	RD
Controls Cerebellar volume	0.35	−0.18	−0.22	0.32	−0.15	0.04
Survivors Cerebellar volume	0.20	−0.07	0.01	−0.15	0.43*	−0.49**
Survivors Cerebellar volume (controlling for NPS)	0.15	−0.02	0.02	−0.04	0.42*	−0.41*
Survivors Cerebellar volume (controlling for NPS and Age at diagnosis)	0.27	−0.03	0.07	−0.10	0.47*	−0.45*

Note. Reported values are Pearson correlation coefficients; *indicates p < .05 and **indicates p < .01; for all significant correlations, adjusted FDR based on Benjamini-Hochberg statistical correction ≤0.01; NPS = neurological predictor scale; FA = fractional anisotropy; RD = radial diffusivity.

hypothesized relationships reflecting a pattern of cascading damage, and instead appear to reflect a correlational pattern of a focal relationship between thalamic-frontal WMI and cerebellar volume in the survivor group. Alternatively, it is possible that the measurement techniques employed by the current study could be insensitive to some segments of the cascade.

Cerebellar atrophy was expected to be negatively correlated with each segment of cerebellar-frontal WMI (cerebellar-rubral, rubral-thalamic, and thalamic-frontal) in the survivor group. As reported in Table 5, Pearson correlations revealed a high correlation between survivors' cerebellar-rubral RD and cerebellar atrophy, indicating that as cerebellar atrophy increased, cerebellar-rubral WMI decreased (see Table 5). While there was a general trend that the portions of the white matter pathway closest to the cerebellum demonstrated slightly higher correlations with cerebellar atrophy, the relationships among the other portions of the pathway did not reach statistical significance (e.g., rubral-thalamic; see Table 5). Correlations were also computed for cerebellar lesion size (hand drawn by neuroradiologist as described by Ailion et al., 2016) and each portion of the cerebellar-frontal pathway; however, none of these results reached statistical significance.

To further investigate these findings, the survivor group was split into radiation and no-radiation groups (see Table 6). In the radiation group, significant correlations were found between each brain structure's regional volume and the thalamic-frontal segment of the pathway. In contrast, the volume of each structure along the pathway was associated with the cerebellar-rubral segment in the no-radiation group. Differences in the radiation and no-radiation group are likely due to the type of brain injury associated with each treatment. In the no-radiation group, the primary mechanisms of injury were cerebellar tumor growth, resection, and hydrocephalus. Therefore, the most proximal connection to that injury (cerebellar-rubral pathway) explained reductions in brain structure volume along the pathway. The radiation group had a multifactorial brain injury from brain surgery and cranial radiation treatment. Cranial radiation treatment is theorized to have the greatest impact on the latest myelinating pathway of the cerebellar-frontal pathway (i.e., thalamic-frontal). Therefore, the initial injury to the thalamic-frontal white matter and failure to attain typical white matter growth may explain reductions of brain structure volume along the pathway. Arguably, the radiation and no-radiation groups had a similar degree and pattern of initial damage. However, subsequent radiation-induced demyelination of the thalamic-frontal portion of the pathway appears to demonstrate a stronger correlational relationship with brain volume loss in the cerebellum, red nucleus, thalamus, and frontal lobe.

To further investigate this theory, a correlation was run between cerebellar-frontal WMI and age at diagnosis for both groups. In the radiation group, age at diagnosis was associated with cerebellar-frontal WMI (FA, $r(14) = 0.52$, $p < .05$; RD, $r(14) = -0.50$, $p = .06$). In contrast, a significant relationship was not found in the no-radiation group (FA $r(13) = 0.40$, $p = .16$; RD $r(13) = 0.06$, $p = .85$).

Pathway specificity in the context of global brain changes is an important consideration in the context of brain tumors given the body of research that documents global changes in this population. To address concerns about specificity in the context of whole brain changes, an analysis was conducted to look at the correlation between cerebellar volumes and whole brain white matter volume to demonstrate specificity of the effects reported (see Table 7). These analyses provide evidence that cerebellar volumes are specific to the cerebellar-frontal pathway and are not related to other white matter pathways in the brain, which are not connected to the cerebellum.

4. Discussion

The white matter pathway connecting the cerebellum and the frontal lobe is commonly studied in the childhood brain tumor population (Ailion et al., 2017). The current study advances the existing literature on this pathway in a variety of ways. The results elucidate the component white matter segments of the cerebellar-frontal pathway, microstructural white matter changes within the cerebellar-frontal pathway, and possible correlational support for transneural degeneration, using deterministic tractography, diffusion-based scalar metrics, and volumetric morphometry, respectively. Relationships among measures of WMI do not reflect cascading damage as initially hypothesized, but instead suggest correlational evidence for focal areas of structural vulnerability. First, only the thalamic-frontal segment of the cerebellar-frontal pathway was associated with the volumetric measures of each structure in the survivor group (see Fig. 3 and Table 4). Second, cerebellar atrophy was only associated with the cerebellar-rubral segment of the cerebellar-frontal pathway (the most proximal segment). This correlational pattern of results provides some evidence that the mechanisms of structural disconnection were more nuanced than initially hypothesized, suggesting possible areas of focal structural vulnerability that may be related to type of brain tumor treatment.

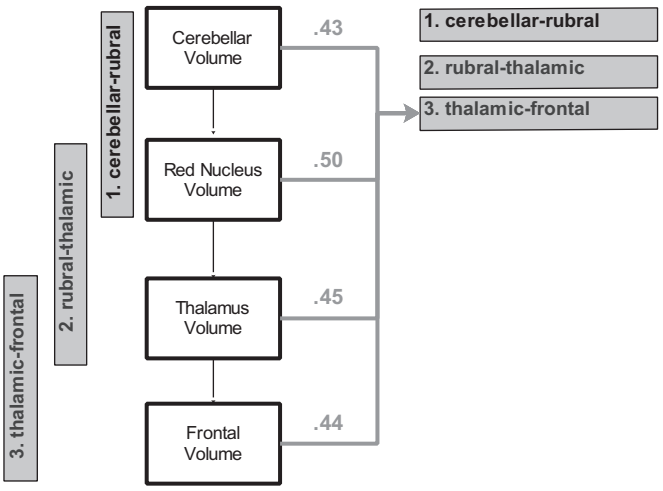

Fig. 3. Correlations between brain structure volume and white matter fractional anisotropy (FA) for the survivor group.
Note. Values are Pearson correlation coefficients without any control variables between volume (white + grey matter divided by intracranial vault) and white matter integrity (thalamic-frontal FA). White boxes denote volumes, and grey boxes denote white matter integrity.

The disruption of cerebellar-frontal connections is likely due to multifactorial injury related to brain tumor treatment. Given the proximity to the cerebellum, it is possible that the etiology of cerebellar atrophy extends to the cerebellar-rubral pathway. Alternatively, cerebellar atrophy may reduce cerebellar output and cause demyelination within the cerebellar-rubral segment. Evidence from the human and animal literature suggests a combination of these explanations. The initial injuries from tumor growth, surgery, and treatment cause demyelination followed by a negative feedback loop in which the cells, blood vessels, and myelin continue to degenerate over time (Glass et al., 2017; Reddick et al., 2005; Reinhold et al., 1990).

The relationship between volumetric measures and the thalamic-frontal segment specifically may be related to differential developmental trajectories of myelination within the cerebellar-frontal pathway. Consistent with this finding, cerebellar-frontal FA was highly correlated with age at diagnosis for survivors treated with cranial radiation. Research suggests that the cerebellum, pons, and cerebellar peduncles exhibit developmentally early myelination and are present at birth, whereas subcortical and frontal regions continue to myelinate into early adulthood (Gao et al., 2009; Paus et al., 2001; Westlye et al., 2010). The correlations between brain structure volume and WMI in the thalamic-frontal segment may be related to initial injury, structural disconnection beginning with atrophy in the cerebellum, and a failure to develop normal white matter gains in developmentally sensitive

Table 4
Correlations between volumetric measures and the diffusion-based scalar metrics of the segments of the cerebellar-frontal pathway.

	Cerebellar-rubral		Rubral-thalamic		Thalamic-frontal	
	FA	RD	FA	RD	FA	RD
Controls						
Left red nucleus volume	0.12	0.08	−0.32	0.47**		
Left thalamus volume			−0.32	0.48**	−0.05	0.06
Left frontal lobe volume					−0.02	0.07
Survivors						
Left red nucleus volume	0.28	0.03	0.14	−0.24		
Left thalamus volume			0.19	−0.29	0.45*	−0.44*
Left frontal lobe volume					0.44*	−0.41*
Survivors (controlling for NPS)						
Left red nucleus volume	0.26	0.04	0.14	−0.24		
Left thalamus volume			0.20	−0.26	0.44*	−0.42*
Left frontal lobe volume					0.43*	−0.39*
Survivors (controlling for NPS and age at diagnosis)						
Left red nucleus volume	0.40*	0.03	0.20	−0.31		
Left thalamus volume			0.26	−0.34	0.49*	−0.46*
Left frontal lobe volume					0.47*	−0.43*

Note. Reported values are Pearson correlation coefficients; *indicates $p < .05$ and **indicates $p < .01$; for all significant correlations, for all significant correlations, adjusted FDR based on Benjamini-Hochberg statistical correction ≤0.01; NPS = neurological predictor scale; FA = fractional anisotropy; RD = radial diffusivity.

regions (Glass et al., 2017; Reddick et al., 2005; Reinhold et al., 1990).

This is the only known study to date that simultaneously investigated the individual segments of the multi-synaptic cerebellar-frontal pathway and the regional volume of the brain structures along this pathway. The current study found that in the no-radiation group the cerebellar-rubral segment correlated with cerebellar, red nucleus, thalamic, and frontal volumes, whereas in the radiation treatment group the thalamic-frontal segment instead correlated with the aforementioned volumes. These results are theoretically meaningful because the no-radiation group showed a correlational pattern that is consistent with theories of structural changes such as transneural degeneration (Deleglise et al. 2017) that underlie diaschisis (von Monakow, 1914). In contrast, the radiation group showed a correlational pattern is consistent with theories of neurodevelopmental vulnerability to radiation-induced demyelination (Palmer et al., 2002; Qiu et al., 2007; Reddick et al., 2000; Reddick et al., 2005; Reinhold et al., 1990; Stevens et al., 2009). These findings would have been impossible to detect without combining imaging techniques (tractography and VBM) and dividing the frontal-cerebellar pathway into meaningful, individual segments. The results also further highlight that more research is needed into the mechanisms underlying distinct brain-behavior relationships. The results of the current study provide a strong justification for investigating complementary multimodal neuroimaging methods in general, and specifically with complex neurological populations.

The current study is among the first to consider the component segments of the cerebellar-frontal pathway, a multi-synaptic white matter pathway that encompasses connections among multiple brain regions. A large number of prior studies on this population have investigated the cerebellar-frontal pathway as a single entity (Law et al., 2011, 2012; Rueckriegel et al., 2015; Soelva et al., 2013). Only two prior studies with this population have parsed the individual white matter segments that directly connect brain structures along the cerebellar-frontal pathway (Law et al., 2015a, 2015b). However, of the aforementioned studies, Law et al. (2015b) looked at medulloblastoma survivors on average 6.28 years post-diagnosis and Law et al. (2015a) only looked at high-grade tumors. Therefore, the current study is the first to segment the cerebellar-frontal pathway in long-term survivors (M = 13 years post diagnosis) using a sample that includes both low and high grade tumors.

Brain tumor populations are difficult to study due to differences in the speed of tumor growth, the age of tumor identification, pathology, and location of the tumor within the posterior fossa. In this population, there was damage to dentate nucleus and cerebellum due to surgical resection. Therefore, heterogeneity among tumor and treatment factors could have contributed to the results. The current study statistically accounted for the influence of treatment factors to ensure that tumor and treatment factors do not better explain the results. Sample size limited the number of treatment factors that could be included as covariates; therefore, NPS was investigated as a cumulative measure of disease severity. The current study had a large number of participants for this patient population of long-term survivors of childhood brain tumors on average 13 years post diagnosis. While it would be desirable to replicate findings with a larger and more homogenous sample, it is challenging to follow brain tumor survivors this long post diagnosis due

Table 5
Correlations between cerebellar atrophy or lesion size and the diffusion-based scalar metrics for segments of the cerebellar-frontal pathway.

	Cerebellar-Rubral		Rubral-Thalamic		Thalamic-Frontal	
	FA	RD	FA	RD	FA	RD
Cerebellar atrophy	−0.32	0.53**	0.22	−0.04	−0.04	−0.01
Cerebellar lesion size (controlling for NPS)	−0.08	0.07	0.06	−0.12	0.20	−0.32
Cerebellar atrophy	−0.30	0.52**	0.22	−0.10	0.06	−0.08
Cerebellar lesion size (controlling for NPS + age at diagnosis)	−0.10	0.09	0.06	−0.09	0.19	−0.30
Cerebellar atrophy	−0.31	0.52**	0.24	−0.12	0.07	−0.09
Cerebellar lesion size	−0.17	0.10	0.03	−0.05	0.17	−0.28

Note. *indicates $p < .05$ and **indicates $p < .01$; Pearson r values are reported; for all significant correlations, adjusted FDR based on Benjamini-Hochberg statistical correction ≤0.01; NPS = neurological predictor scale; FA = fractional anisotropy; RD = radial diffusivity.

Table 6
Radiation subgroup comparisons for the cerebellar-frontal pathway.

	Cerebellar-Frontal		Cerebellar-Rubral		Rubral-Thalamic		Thalamic-Frontal	
	FA	RD	FA	RD	FA	RD	FA	RD
No radiation (n = 14)								
Right cerebellum volume	0.58*	−0.28	0.59*	−0.15	−0.26	−0.26	0.28	−0.44
Left red nucleus volume	0.72**	−0.13	0.64*	−0.04	−0.07	−0.28	0.41	−0.45
Left thalamus volume	0.66**	−0.26	0.50	−0.21	0.07	−0.36	0.35	−0.31
Left frontal lobe volume	0.65*	−0.18	0.56*	−0.11	−0.07	−0.33	0.38	−0.45
Radiation (n = 15)								
Right cerebellum volume	0.20	−0.06	−0.20	0.00	0.26	−0.02	0.60*	−0.46
Left red nucleus Volume	0.28	−0.13	−0.13	0.11	0.33	−0.26	0.58*	−0.58*
Left thalamus volume	0.30	−0.17	−0.07	0.08	0.33	−0.30	0.55*	−0.55*
Left frontal lobe volume	0.29	−0.14	−0.08	0.08	0.29	−0.24	0.50	−0.44

Note. *indicates $p < .05$ and **indicates $p < .01$; reported values are Pearson correlation coefficients; FA = fractional anisotropy; RD = radial diffusivity; Radiation therapy was coded as dichotomous variables in which 0 = not present and 1 = present.

Table 7
Specificity analyses.

	Whole brain white matter volume
Controls Cerebellar volume	$r = 0.20$, $p = .30$
Survivors Cerebellar volume	$r = -0.20$, $p = .31$
Survivors Cerebellar volume (controlling for NPS)	$r = -0.26$, $p = .19$
Survivors Cerebellar volume (controlling for NPS and Age at diagnosis)	$r = -0.19$, $p = .33$
Survivors Radiation group Cerebellar volume	$r = 0.14$, $p = .46$
Survivors No radiation group Cerebellar volume	$r = -0.12$, $p = .70$

to difficulties tracking patients over time and across their transition into adulthood.

While the present study focused on the right cerebellar-left frontal pathway based on the evidence that this pathway is related to executive functioning (Law et al., 2015b), prior research has found that damage also exists in the contralateral pathway for this population (e.g., Rueckriegel et al., 2015; Law et al., 2015a). However, there is value to knowing more about this contralateral pathway and verifying that there is no relationship between it and executive function measures. In particular, the lack of a correlation would verify that the lack of a left-cerebellum – right-frontal correlation is not unique to the sample of the previous (Law et al., 2015b) study. Future research should investigate a more comprehensive study of bilateral tracks to better understand the neuroanatomical and neuropsychological changes following brain tumor treatment. Future researchers are also encouraged to incorporate more sophisticated neuroimaging metrics that can account for the possible warping in frontal lobes due to AP encoding.

The results of the current study are critical to advancing the understanding of structural brain changes following brain tumor treatment. These results are clinically useful for educating families of posterior fossa tumor survivors about the relationships among affected brain regions and affected pathways. These results are of particular relevance because researchers have begun to apply region-based, volumetric measures to the clinical interpretation of brain MRIs (e.g., Bigler, 2016). Therefore, it is increasingly critical to understand how measures of regional brain structure volume relate to other complementary neurobiological markers (e.g., WMI) in clinical populations.

Acknowledgements

We would like to express our gratitude to the individuals and families who participated in this study and generously contributed their time and effort. We would also like to acknowledge the Developmental Neuropsychology across the Lifespan Research Team for helping with data acquisition and management and the Brain Tumor Foundation for helping share information about this clinical research opportunity with long-term brain tumor survivors. We thank the anonymous peer reviewers for their thoughtful and helpful comments to improve this work.

Funding sources

This research was supported by a Research Scholar Grant from the American Cancer Society to TZK (#RSGPBCPPB-114044). AA was supported by a doctoral fellowship provided by the Georgia State University Language and Literacy Initiative.

Appendix A. Appendix

A.1. ROI Procedures

A.1.1. Right cerebellum

The right cerebellum was drawn beginning with the lateral-most coronal slice where the cerebellum could be identified. The superior portion of the cerebellum was defined using the cerebellar tentorium as a guide. The pons was used as the anterior boundary, and the midline of the cerebellar vermis was used to delineate the left boundary of the ROI.

A.1.2. Right dentate

The dentate was identified as a grey matter structure that was surrounded by white matter. The dentate was drawn beginning with the brainstem in the axial view, and the midline of the cerebellum in the sagittal and coronal view. The ROI mask was placed over the crescent-shaped figure in the middle of the cerebellar white matter in the right hemisphere. This mask was drawn to include 1–2 voxels of white matter along the grey matter borders, to ensure the mask would capture the dentate connections to white matter pathways that continue to the cortex.

A.1.3. Left red nucleus

The left red nucleus was identified by selecting the anterior-most

midbrain slice in which it becomes visible in the axial view, using the cerebral peduncles and substantia nigra as anterior and posterior reference points, respectively. For this structure the T2 image was also used as a guide, as the red nucleus appears grey on T2 images due to iron composition. Similar to the dentate mask, this mask was drawn to include a 1–2 voxel border into the white matter. For neuroanatomical reference, see page Fig. 6.10B on page 234 of Blumenfeld (2010).

A.1.4. Left thalamus

The massa intermedia or lateral ventricles as relevant defined the right boundary of the thalamus. The posterior internal capsule defined the left boundary of the thalamus. The anterior boundary was defined using the differentiation between the grey matter of the thalamus and surrounding white matter of the internal capsule. Dorsal and ventral boundaries were based on continuous slices of the differentiation between the grey and white matter boundaries on the T1 images, with the posterior commissure as another reference point for the ventral boundary. For neuroanatomical reference points, please see Fig. 10-19B on page 144 of Waxman (2009).

A.1.5. Left middle frontal gyrus (MFG)

The anterior boundary of the left MFG was defined as the anterior portion of the superior frontal sulcus, and the posterior portion was defined by the caudal part of the middle frontal gyrus. The superior frontal sulcus was defined by the dorsal boundary, and the ventral boundary of the MFG was defined as the inferior frontal sulcus.

A.1.6. Reduced size MFG

The left MFG was reduced in size, after delineation, for efficient network processing. Specifically, the masks used for processing included the first 10-slices of the anterior portion of the MFG. The reduction of the size of the MFG was modeled after the ROI slice procedure described by Ford et al. (2013). While one could argue that a larger ROI is more precise and includes more fiber estimations, it could also be argued that smaller, more precise ROI boundaries increase neuroanatomical specificity. The use of PanTrack for network tractography both between and within structures addresses some of these concerns by decreasing reliance on ROI boundaries while maintaining the specificity of between-structure networking methods. To date, all prior studies using MOW reconstruction and direct structural networking have only used between-structure networking. Even with a reduced size ROI for the MFG, this method is far superior to prior studies that have used a single slice estimate of ROIs (Jissendi et al., 2008), or defined the frontal ROI too broadly as the dorsal anterior half of the cortex (Law et al., 2015a).

A.1.7. ROI template method

The method of ROI template generation was based on Law et al. (2015a), which involved manually drawing the ROIs on 10 healthy controls, registering the ROIs to the standard MNI (Montreal Neurological Institute) ICBM152 brain to create an ROI template, then registering the template to each participant's native space, and manually editing when necessary (Woods et al., 1998; http://bishopw.loni.ucla.edu/air5). While this technique was successful in a brain tumor population in one prior study (Law et al., 2015a), one possible limitation of this approach was the potential inaccuracies when converting the template image from standard MNI152 space to native space, due to structural brain abnormalities (e.g., lesions from surgical resection, inter-individuals in sulcal anatomy; Ono et al., 1990). However, a systematic semi-automated approach to ROI reduces the time intensive nature of manual ROI drawings and provides a more objective and standardized approach to ROI generation.

Ten (10) healthy controls were randomly selected to develop the ROI templates. The regions of interest were drawn on the FA image for each control, and co-registered T1 images were used as an anatomical guide. All ROIs were delineated by referencing anatomical guidelines provided by neuroanatomical atlases (e.g., Naidich et al., 2009). Then, all images and ROIs were co-registered to the MNI152 brain template. Once all images were in MNI space, each of the ROIs was combined across participants to obtain an average ROI template across the 10 randomly selected controls. Each of these ROI templates was then visually verified and manually edited when necessary to be consistent with the aforementioned ROI boundaries on the MNI152 brain to create the template ROIs.

Next, AFNI's non-linear registration program was used (Cox, 1996; Cox and Jesmanowicz, 1999) to register each participant's FA image to the standard MNI152 FA image (1x1x1mm). Following registration, AFNI was used to calculate the inverse normalization warp matrix from MNI152 space to native space. The inverse matrix was then applied to the template ROIs to bring the template ROIs into native space for each participant. Once the ROIs were in native space, each ROI was checked for accuracy. This method was used for all the ROI templates. In general, the template ROIs registered accurately to the participants' native space based on a visual investigation of the images, and ROIs were manually corrected when necessary. All ROIs were carefully checked and edited after each transformation.

References

Ailion, A.S., King, T.Z., Wang, L., Fox, M.E., Mao, H., Morris, R.M., Crosson, B., 2016. Cerebellar atrophy in adult survivors of childhood cerebellar tumor. J. Int. Neuropsychol. Soc. 1–11. https://doi.org/10.1017/s1355617716000138.

Ailion, A.S., Hortman, K., King, T.Z., 2017. Childhood brain Tumors: a systematic review of the structural neuroimaging literature. Neuropsychol. Rev. 1–25 E-pub before print.

Alexander, G.E., DeLong, M.R., Strick, P.L., 1986. Parallel organization of functionally segregated circuits linking basal ganglia and cortex. Annu. Rev. Neurosci. 9, 357–381. https://doi.org/10.1146/annurev.ne.09.030186.002041.

Andersen, B.B., Korbo, L., Pakkenberg, B., 1992. A quantitative study of the human cerebellum with unbiased stereological techniques. J. Comp. Neurol. 326 (4), 549–560. https://doi.org/10.1002/cne.903260405.

Benjamini, Y., Hochberg, Y., 1995. Controlling the false discovery rate: a practical and powerful approach to multiple testing. J. R. Stat. Soc. 57 (1), 289–300. https://doi.org/10.2307/2346101.

Bennett, C.M., Wolford, G.L., Miller, M.B., 2009. The principled control of false positives in neuroimaging. Soc. Cogn. Affect. Neurosci. 4, 417–422. https://doi.org/10.1093/scan/nsp053.

Bigler, E.D., 2016, February. Clinical Application of Individualized Quantitative Neuroimaging for Neuropsychology – Precision Medicine Meets Neurocognitive Assessment. Oral presentation at the annual meeting of the International Neuropsychological Society, Boston, MA.

Blumenfeld, H., 2010. Neuroanatomy through Clinical Cases, 2nd edition. Sinauer Associates, Inc. (ISBN 978-0-87893).

Brodmann K. Vergleichende lokalisationslehre der großhirnrinde: In ihren prinzipien. Leipzig, Germany: Barth, 1909.

Bohsali, A., Triplett, W., Sudhyadhom, A., Gullett, J.M., McGregor, K., FitzGerald, D.B., Crosson, B., 2015. Broca's area - Thalamic connectivity. Brain and Language 141C, 80–88. https://doi.org/10.1016/j.bandl.2014.12.001.

Catani, M., Dell'acqua, F., Vergani, F., Malik, F., Hodge, H., Roy, P., 2012. Thiebaut de Schotten, M. Short frontal lobe connections of the human brain. Cortex 48 (2), 273–291. https://doi.org/10.1016/j.cortex.2011.12.001.

Colon-Perez, L.M., Spindler, C., Goicochea, S., Triplett, W., Parekh, M., Montie, E., Mareci, …., H, T., 2015. Dimensionless, Scale Invariant, Edge Weight Metric for the Study of Complex Structural Networks. Plos One 10 (7), 1–29. https://doi.org/10.1371/journal.pone.0131493.

Deleglise, B., Lassus, B., Soubeyre, V., Doulazmi, M., Brugg, B., Vanhoutte, P., Peyrin, J.-M., 2018. Dysregulated Neurotransmission induces Trans-synaptic degeneration in reconstructed Neuronal Networks. Sci. Rep. 8 (1), 11596. https://doi.org/10.1038/s41598-018-29918-1.

Desikan, R.S., Segonne, F., Fischl, B., Quinn, B.T., Dickerson, B.C., Blacker, D., Killiany, R.J., 2006. An automated labeling system for subdividing the human cerebral cortex on MRI scans into gyral based regions of interest. Neuroimage 31 (3), 968–980. https://doi.org/10.1016/j.neuroimage.2006.01.021.

Dietrich, U., Wanke, I., Mueller, T., Wieland, R., Moellers, M., et al., 2001. White matter disease in children treated for malignant brain tumors. Childs Nerv. Syst. 17, 731–738.

Duffner, P.K., 2004. Long-term effects of radiation therapy on cognitive and endocrine function in children with leukemia and brain tumors. Neurologist 10 (6), 293–310. https://doi.org/10.1097/01.nrl.0000144287.35993.96.

Eisen, A., Weber, M., 2001. The motor cortex and amyotrophic lateral sclerosis. Muscle Nerve 24 (4), 564–573. https://doi.org/10.1002/mus.1042.

Ford, A., Colon-Perez, L., Triplett, W.T., Gullett, J.M., Mareci, T.H., Fitzgerald, D.B., 2013. Imaging white matter in human brainstem. Front. Hum. Neurosci. 7 (July), 400. https://doi.org/10.3389/fnhum.2013.00400.

Gao, W., Lin, W., Chen, Y., Gerig, G., Smith, J.K., Jewells, V., Gilmore, J.H., 2009. Temporal and spatial development of axonal maturation and myelination of white matter in the developing brain. AJNR Am J Neuroradiol 30 (2), 290–296. https://doi.org/10.3174/ajnr.A1363.

Glass, J.O., Ogg, R.J., Hyun, J.W., Harreld, J.H., Schreiber, J.E., Li, Y., Reddick, W.E., 2017. Disrupted development and integrity of frontal white matter in patients treated for pediatric medulloblastoma. Neuro-Oncology. https://doi.org/10.1093/neuonc/nox062.

Gurney, G.G., Smith, M.A., Bunin, G.R., 1999. CNS and miscellaneous intracranial and intraspinal neoplasms. In: Ries, L., Smith, M., Gurney, J., Linet, M., Tamra, T. (Eds.), Cancer Incidence and Survival among Children and Adolescents: United States SEER Program 1975–1995 (99–4649 Ed.), Retrieved from. http://seer.cancer.gov/publications/childhood/cns.pdf.

Herculano-Houzel, S., 2009. The human brain in numbers: a linearly scaled-up primate brain. Front. Hum. Neurosci. 3, 31. https://doi.org/10.3389/neuro.09.031.2009.

Jian, B., Vemuri, B.C., Özarslan, E., Carney, P.R., Mareci, T.H., 2007. A novel tensor distribution model for the diffusion-weighted MR signal. NeuroImage 37 (1), 164–176. https://doi.org/10.1016/j.neuroimage.2007.03.074.

Jian, B., Vemuri, B.C., 2007a. A unified computational framework for deconvolution to reconstruct multiple fibers from diffusion weighted MRI. IEEE Transactions on Medical Imaging 26 (11), 1464–1471. https://doi.org/10.1109/TMI.2007.907552.

Jian, B., Vemuri, B.C., 2007b. Multi-Fiber Reconstruction from Diffusion MRI Using Mixture of Wisharts and Sparse Deconvolution. Inf Process Med Imaging. 20, 384–395.

Jissendi, P., Baudry, S., Baleriaux, D., 2008. Diffusion tensor imaging (DTI) and tractography of the cerebellar projections to prefrontal and posterior parietal cortices: a study at 3T. J. Neuroradiol. 35, 42–50.

Kelly, R.M., Strick, P.L., 2003. Cerebellar loops with motor cortex and prefrontal cortex of a nonhuman primate. J. Neurosci. Off. J. Soc. Neurosci. 23, 8432–8444.

Khong, P.L., Kwong, D.L., Chan, G.C., Sham, J.S., Chan, F.L., Ooi, G.C., 2003. Diffusion-tensor imaging for the detection and quantification of treatment-induced white matter injury in children with medulloblastoma: a pilot study. AJNR Am. J. Neuroradiol. 24 (4), 734–740.

King, T.Z., Wang, L., Mao, H., 2015. Disruption of white matter integrity in adult survivors of childhood brain Tumors: correlates with long-term intellectual outcomes. PLoS One 10 (7), e0131744. https://doi.org/10.1371/journal.pone.0131744.

King, T.Z., Na, S., 2016. Cumulative neurological factors associated with long-term outcomes in adult survivors of childhood brain tumors. Child Neuropsychology : A Journal on Normal and Abnormal Development in Childhood and Adolescence 22 (6), 748–760. https://doi.org/10.1080/09297049.2015.1049591.

Kirschen, M.P., Davis-Ratner, M.S., Milner, M.W., Chen, S.H., Schraedley-Desmond, P., Fisher, P.G., Desmond, J.E., 2008. Verbal memory impairments in children after cerebellar tumor resection. Behav. Neurol. 20 (1–2), 39–53. https://doi.org/10.3233/ben-2008-0216.

Koliatsos, V.E., Dawson, T.M., Kecojevic, A., Zhou, Y., Wang, Y.-F., Huang, K.-X., 2004. Cortical interneurons become activated by deafferentation and instruct the apoptosis of pyramidal neurons. Proc. Natl. Acad. Sci. 101 (39), 14264–14269. https://doi.org/10.1073/pnas.0404364101.

Konczak, J., Schoch, B., Dimitrova, A., Gizewski, E., Timmann, D., 2005. Functional recovery of children and adolescents after cerebellar tumour resection. Brain J. Neurol. 128 (Pt 6), 1428–1441. https://doi.org/10.1093/brain/awh385.

Küper, M., Doring, K., Spangenberg, C., Konczak, J., Gizewski, E.R., Schoch, B., Timmann, D., 2013. Location and restoration of function after cerebellar tumor removal-a longitudinal study of children and adolescents. Cerebellum 12 (1), 48–58. https://doi.org/10.1007/s12311-012-0389-z.

Lange, W., 1975. Cell number and cell density in the cerebellar cortex of man and some other mammals. Cell Tissue Res. 157 (1), 115–124.

Law, N., Bouffet, E., Laughlin, S., Laperriere, N., Briere, M.E., Strother, D., Mabbott, D., 2011. Cerebello-thalamo-cerebral connections in pediatric brain tumor patients: impact on working memory. NeuroImage 56 (4), 2238–2248. https://doi.org/10.1016/j.neuroimage.2011.03.065.

Law, N., Greenberg, M., Bouffet, E., Taylor, M.D., Laughlin, S., Strother, D., Mabbott, D.J., 2012. Clinical and neuroanatomical predictors of cerebellar mutism syndrome. Neuro-Oncology 14 (10), 1294–1303. https://doi.org/10.1093/neuonc/nos160.

Law, N., Greenberg, M., Bouffet, E., Laughlin, S., Taylor, M.D., Malkin, D., Mabbott, D., 2015a. Visualization and segmentation of reciprocal cerebrocerebellar pathways in the healthy and injured brain. Hum. Brain Mapp. 36 (7), 2615–2628. https://doi.org/10.1002/hbm.22795.

Law, N., Smith, M.L., Greenberg, M., Bouffet, E., Taylor, M.D., Laughlin, S., Mabbott, D., 2015b. Executive function in paediatric medulloblastoma: the role of cerebrocerebellar connections. J. Neuropsychol. https://doi.org/10.1111/jnp.12082.

Marvel, C.L., Desmond, J.E., 2010. The contributions of cerebro-cerebellar circuitry to executive verbal working memory. Cortex 46 (7), 880–895. https://doi.org/10.1016/j.cortex.2009.08.017.

Micklewright, J.L., King, T.Z., Morris, R.D., Krawiecki, N., 2008. Quantifying pediatric neuro-oncology risk factors: development of the neurological predictor scale. J. Child Neurol. 23 (4), 455–458. https://doi.org/10.1177/0883073807309241.

Morris, E.B., Phillips, N.S., Laningham, F.H., Patay, Z., Gajjar, A., Wallace, D., ... Ogg, R.J., 2009. Proximal dentatothalamocortical tract involvement in posterior fossa syndrome. Brain J. Neurol. 132 (Pt 11), 3087–3095. https://doi.org/10.1093/brain/awp241.

Mueller, S., Chang, S., 2009. Pediatric brain tumors: current treatment strategies and future therapeutic approaches. Neurotherapeutics: The journal of the American Society for Experimental NeuroTherapeutics 6 (3), 570–586. https://doi.org/10.1016/j.nurt.2009.04.006.

Naidich, T.P., Duvernoy, H.M., Delman, B.N., Sorensen, A.G., Kollias, S.S., Haacke, E.M., 2009. Duvernoy's Atlas of the Human Brain Stem and Cerebellum High-Field MRI: Surface Anatomy, Internal Structure, Vascularization and 3D Sectional Anatomy. Springer, Wien, Austria.

Nejat, F., Khashab, M.E., Rutka, J.T., 2008. Initial management of childhood brain tumors: neurosurgical considerations. J. Child Neurol. 23 (10), 1136–1148. https://doi.org/10.1177/0883073808321768.

Ono, M., Kubik, S., Abernathey, C.D., 1990. Atlas of the Cerebral Sulci. Thieme, New York.

Ostrom, Q.T., de Blank, P.M., Kruchko, C., Petersen, C.M., Liao, P., Finlay, J.L., ... Barnholtz-Sloan, J.S., 2015. Alex's lemonade stand foundation infant and childhood primary brain and central nervous system tumors diagnosed in the United States in 2007-2011. Neuro-oncology 16 (Suppl. 10), x1–x36. https://doi.org/10.1093/neuonc/nou327.

Palmer, S.L., Reddick, W.E., Glass, J.O., Gajjar, A., Goloubeva, O., Mulhern, R.K., 2002. Decline in corpus callosum volume among pediatric patients with medulloblastoma: longitudinal MR imaging study. AJNR Am. J. Neuroradiol. 23 (7), 1088–1094.

Parent, A., 1996. Carpenter's Human Neuroanatomy. Williams and Wilkins, Media, PA.

Paus, T., Collins, D.L., Evans, A.C., Leonard, G., Pike, B., Zijdenbos, A., 2001. Maturation of white matter in the human brain: a review of magnetic resonance studies. Brain Res. Bull. 54, 255–266. https://doi.org/10.1016/S0361-9230(00)00434-2.

Pinching, A.J., Powell, T.P.S., 1971. Ultrastructure features of transneuronal cell degeneration in the olfactory system. J.Cell Sci. 8 (1964), 253–287.

Puget, S., Boddaert, N., Viguier, D., Kieffer, V., Bulteau, C., Garnett, M., Grill, J., 2009. Injuries to inferior vermis and dentate nuclei predict poor neurological and neuropsychological outcome in children with malignant posterior fossa tumors. Cancer 115 (6), 1338–1347. https://doi.org/10.1002/cncr.24150.

Qiu, D., Kwong, D.L.W., Chan, G.C.F., Leung, L.H.T., Khong, P.L., 2007. Diffusion tensor magnetic resonance imaging finding of discrepant fractional anisotropy between the frontal and parietal lobes after whole-brain irradiation in childhood medulloblastoma survivors: reflection of regional white matter radiosensitivity? International Journal of Radiation Oncology • Biology • Physics 69 (3), 846–851. https://doi.org/10.1016/j.ijrobp.2007.04.041.

Reddick, W.E., Russell, J.M., Glass, J.O., et al., 2000. Subtle white matter volume differences in children treated for medulloblastoma with conventional or reduced-dose cranial-spinal irradiation. Magn. Reson. Imaging 18, 787–793.

Reddick, W.E., Glass, J.O., Palmer, S.L., Wu, S., Gajjar, A., Langston, J.W., Mulhern, R.K., 2005. Atypical white matter volume development in children following craniospinal irradiation. Neuro-oncology 7 (1), 12–19. https://doi.org/10.1215/S1152851704000079.

Rehme, A.K., Grefkes, C., 2013. Cerebral network disorders after stroke: evidence from imaging-based connectivity analyses of active and resting brain states in humans. J. Physiol. 591 (1), 17–31. https://doi.org/10.1113/jphysiol.2012.243469.

Reinhold, H.S., Calvo, W., Hopewell, J.W., Van Den Breg, A.P., 1990. Development of blood vessel-related radiation damage in the fimbria of the central nervous system. International Journal of Radiation Oncology Biology Physics 18, 37–42.

Roberts, S., 2017. Structural connectivity of the inferior frontal gyrus, thalamus, and basal ganglia in healthy young adults (Unpublished master's thesis. Georgia State University, Atlanta, GA.

Rueckriegel, S.M., Bruhn, H., Thomale, U.W., Hernaiz Driever, P., 2015. Cerebral white matter fractional anisotropy and tract volume as measured by MR imaging are associated with impaired cognitive and motor function in pediatric posterior fossa tumor survivors. Pediatr. Blood Cancer 62 (7), 1252–1258. https://doi.org/10.1002/pbc.25485.

Soelva, V., Hernaiz Driever, P., Abbushi, A., Rueckriegel, S., Bruhn, H., Eisner, W., Thomale, U.W., 2013. Fronto-cerebellar fiber tractography in pediatric patients following posterior fossa tumor surgery. Child's Nervous Systemy 29 (4), 597–607. https://doi.org/10.1007/s00381-012-1973-8.

Spanos, G.K., Wilde, E.A., Bigler, E.D., Cleavinger, H.B., Fearing, M.A., Levin, H.S., ... Hunter, J.V., 2007. Cerebellar atrophy after moderate-to-severe pediatric traumatic brain injury. Am. J. Neuroradiol. 28, 537–542.

Stevens, M.C., Skudlarski, P., Pearlson, G.D., Calhoun, V.D., 2009. Age-related cognitive gains are mediated by the effects of white matter development on brain network integration. Neuroimage 48 (4), 738–746. https://doi.org/10.1016/j.neuroimage.2009.06.065.

Szathmari, A., Thiesse, P., Galand-desmé, S., et al., 2010. Correlation between pre- or postoperative MRI findings and cerebellar sequelae in patients with medulloblastomas. Pediatr. Blood Cancer 55 (7), 1310–1316.

Taiwo, Z., Na, S., King, T.Z., 2017. The Neurological Predictor Scale: A predictive tool for neurocognitive late effects in survivors of childhood brain tumors. Pediatric Blood and Cancer 64 (1), 172–179. https://doi.org/10.1002/pbc.26203.

von Monakow, C., 1914. Die Localization im Grosshirn und der Abbau der Funktion durch korticale Herde. JF Bergmann, Wiesbaden, Germany.

Turken, A.U., Dronkers, N.F., 2011. The neural architecture of the language comprehension network: converging evidence from lesion and connectivity analyses. Front Syst Neurosci 5 (1). https://doi.org/10.3389/fnsys.2011.00001.

Waxman, S.G., 2009. Clinical neuroanatomy. McGraw-Hill Education, New York.

Westlye, L.T., Walhovd, K.B., Dale, A.M., Bjornerud, A., Due-Tonnessen, P., Engvig, A., Fjell, A.M., 2010. Life-span changes of the human brain white matter: diffusion tensor imaging (DTI) and volumetry. Cereb. Cortex 20 (9), 2055–2068. https://doi.org/10.1093/cercor/bhp280.

Whiting, B.A., Barton, R.A., 2003. The evolution of the cortico-cerebellar complex in primates: anatomical connections predict patterns of correlated evolution. J. Hum. Evol. 44 (1), 3–10.

Woods, R.P., Grafton, S.T., Holmes, C.J., Cherry, S.R., Mazziotta, J.C., 1998. Automated image registration: I. general methods and intrasubject, intramodality validation. J. Comput. Assist. Tomogr. 22, 139–152.

Zhang, J.X., Leung, H.C., Johnson, M.K., 2003. Frontal activations associated with accessing and evaluating information in working memory: An fMRI study. Neuroimage 20 (3), 1531–1539.

Zhang, Y., Zou, P., Mulhern, R.K., Butler, R.W., Laningham, F.H., Ogg, R.J., 2008. Brain structural abnormalities in survivors of pediatric posterior fossa brain tumors: a voxel-based morphometry study using free-form deformation. NeuroImage 42 (1), 218–229. https://doi.org/10.1016/j.neuroimage.2008.04.181.